(2)

# *Fairfax Materials Research Inc.*

**5613 Marble Arch Way**
**Alexandria, Virginia 22310-4011**

**(703)-922-4579 Fax: (703)-922-6034**

June 14 1993

Dr. A. K. Vasudevan, code 1222
Office of Naval Research
800 N. Quincy Street
Arlington, VA 22217-5000

re: Contract #N00014-91-C-0067

Dear Dr. Vasudevan:

Please find attached one copy of the May 16 report on the above contract, as specified in your letter of August 7, 1992 (your ref: 3900 Ser 1222/01) and in accordance with the contract above.

Work during this last quarter has centered on PZT and its properties.

Yours sincerely

Dr. M.S. Duesbery
Vice-President
Fairfax Materials Research, Inc.



cc: ACO
NRL
DTIC (2)

# Computer Modelling of Cyclic Deformation of High-Temperature Materials

**TECHNICAL PROGRESS REPORT**

Dr. M.S. Duesbery
***Principal Investigator***

Dr. N.P. Louat
***Senior Scientist***

## Fairfax Materials Research, Inc.
**5613 Marble Arch Way**
**Alexandria, VA 22310-4011**

June 14, 1993

Period of performance
February 1, 1993 through May 31, 1993

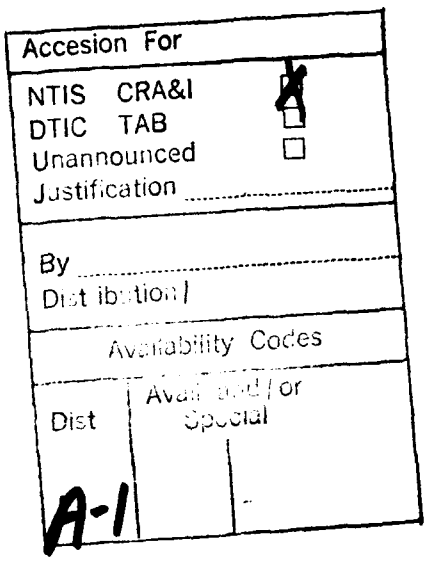




Statement A per telecon Asuni Vasudevan
ONR/Code 1222
Arlington, VA 22217-5000

NWW 12/15/93

# I. Introduction and Program Objective

Current methods of lifetime assessment leave much to be desired. Typically, the expected life of a full-scale component exposed to a complex environment is based upon empirical interpretations of measurements performed on microscopic samples in controlled laboratory conditions. Extrapolation to the service component is accomplished by scaling laws which, if used at all, are empirical; little or no attention is paid to synergistic interactions between the different components of the real environment. With the increasingly hostile conditions which must be faced in modern aerospace applications, improvement in lifetime estimation is mandated by both cost and safety considerations.

This program aims at improving current methods of lifetime assessment by building in the characteristics of the micro-mechanisms known to be responsible for damage and failure. The broad approach entails the integration and, where necessary, augmentation of the micro-scale research results currently available in the literature into a macro-scale model with predictive capability.

In more detail, the program will develop a set of hierarchically structured models at different length scales, from atomic to macroscopic, at each level taking as parametric input the results of the model at the next smaller scale. In this way the known microscopic properties can be transported by systematic procedures to the unknown macro-scale region. It may not be possible to eliminate empiricism completely, because some of the quantities involved cannot yet be estimated to the required degree of precision. In this case the aim will be at least to eliminate functional empiricism. Restriction of empiricism to the choice of parameters to be input to known functional forms permits some confidence in extrapolation procedures and has the advantage that the models can readily be updated as better estimates of the parameters become available.

# II. Program Organization

The program has been organized into specific tasks and subtasks as follows.

**Task 100. Lifetimes of metallic dispersed-phase composites**

Most service materials fall into the category of dispersion-hardened metallic composites. This task will consider the problem of dispersion hardened materials in general, but with two specific materials, NiAl and $MoSi_2$/SiC in mind.

**Task 110. Identification and modelling of micromechanisms**

The purpose of this task is to determine what micromechanisms are operative in the high-temperature deformation of dispersion-hardened materials. In the general case this will be done by a literature search. For specific materials, the micromechanisms will be determined from the

experimental program at NRL. Once identified, each of these micromechanisms will be modelled, in order to determine what are the critical parameters which determine its effect on plastic flow and values for these parameters. Also to be determined is whether the modelled critical values are dependent on quantities which must be obtained from a smaller scale model.

### Task 111. Equiaxed dispersoids

This task will consider dispersions of the type encountered in NiAl-like materials. That is, the dispersoids are considered to be small compared to the grain size. The term 'equiaxed' is used because the particles are roughly of the same size in all three dimensions. However, this is not a requirement for this task. Rather, it is necessary that the particles not be too large in the dimension normal to the slip plane, so that they can be surmounted with relative ease by cross-slip and/or climb without the generation of appreciable back-stress.

### Task 112. Anisotropic dispersoids

This task covers the case of dispersoids which are elongated in the direction normal to the slip plane. An example is SiC fibers in $MoSi_2$. In this case, plastic flow around the dispersoids takes place by a combination of glide and climb, but is a protracted process during which large stresses acting in opposition to the applied load are developed.

### Task 113. Grain boundary effects

This task will examine the role of grain boundary processes in high-temperature deformation.

### Task 120. Macroscopic stochastic model for creep

In real materials it is likely that more than one mechanism will be operative, either in parallel or in series. The information gained in task 110 is not sufficient to describe this situation. Once the critical parameters for individual mechanisms have been determined, it is necessary to combine them in a macroscale stochastic model. This will be done by determining critical stresses and activation enthalpies as a function of local geometry and using these values in a finite-temperature simulation of creep through a random array of dispersoids. Careful attention must be paid to possible interactions between mechanisms.

### Task 130. Extension to cyclic deformation

The final step in task 100 is to extend the results to the case of cyclic deformation. Irreversibility is an intrinsic feature of the model in task 120. However, it is likely that other, as yet unrecognized, characteristics of cycled deformation will have to be considered.

**Task 200. Lifetimes of piezoelectric ferroelectrics**

Failure in cyclic loading of sensors and actuators formed from lead zirconate titanate (PZT) is a continuing problem. PZT is a ceramic and therefore differs from the materials considered in task 100 in that plastic deformation is not involved. This task will examine, modelling as necessary, the operation of PZT devices, in order to determine the factors governing lifetime limitation.

**Task 300. Reporting**

Running concurrently with tasks 100 and 200, this task will inform the Navy Program Manager and Contracting Officer of the technical and fiscal status of the program through R&D status reports.

# III. Technical Progress

## Task 100. Lifetimes of metallic dispersed-phase composites
## Task 110. Identification and modelling of micromechanisms

Three publications of varying degrees of relevance to the present program are appended to this report.

"The Flow Stress of Potassium" by Duesbery and Basinski, demonstrates that quantitative agreement between theory and experiment can be obtained at the microscopic level from first principles calculations for sophisticated maechanical properties such as the flow stress.

"Self-Repair of Monolayers with Vacancy Damage" by Joos and Duesbery, introduces a novel and potentially useful property of certain thin coating materials.

"On Hardening by Dispersed Spherical Particles" by Louat and Duesbery, covers the analytic work on dispersion hardening which was detailed in the last report.

## Task 200. Lifetimes of piezoelectric ferroelectrics

The utility of PZT as a 'smart material' is severely limited by its premature mechanical failure when subjected to cyclic loading. The cause of this failure forms the critical question. The central problem is that an irreversible mechanism is necessary to explain the experimental observations, while the overt physical properties - that is, piezoelectricity, ferroelectricity and ferroelasticity - are all symmetric to reversal. A theory will be presented which introduces an intrinsic irreversibility and, at the same time, explains all salient experimental observations. Critical experiments and modelling directions will be detailed.

The key experimental observations are as follows.

⋆In the poled state, ferroelectric domains are elongated strongly in the direction of the poling field and are separated by walls with little curvature.

⋆Under cyclic mechanical loading at 70% of the monotonic fracture stress, the lifetime is in excess of $10^7$ cycles. At stress amplitudes from 75% to 95% of the fracture stress, the lifetime decreases sharply from $10^5$ to $10^2$ cycles)[6]. The effect of temperature is unknown.

⋆Under cyclic (resonant) electrical loading, the lifetime depends on temperature. For deformation above 80° C, failure is much more rapid than below this critical temperature. Predeformation below 80° C prior to high-temperature deformation leads to even more rapid failure. Damage is not detectable for deformation below 80° C, but is observed as intergranular cracking at higher temperatures[6].

## *a. Theory*

### a.1 Domain Wall Motion

There are two regimes of domain wall motion, depending on the domain structure and the misfit strain. For thin domains and/or small misfit, the incommensuracy is accommodated by coherency strains. For thick domains and/or large misfit strain, the domain walls are expected to bind strongly to dislocations. This report will be concerned only with the second regime, in which the domain wall motion is limited by dislocation motion.

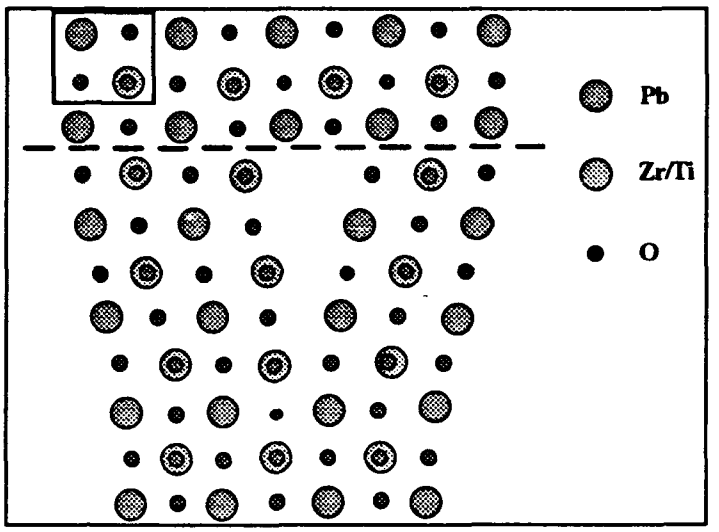


**Figure 1** A domain wall dislocation in PZT

The dislocations of importance will have Burgers vectors and line directions lying in the plane of the domain walls. Motion of the domain walls normal to themselves therefore requires that these dislocations move by climb. In general, dislocation climb is a process requiring the emission or absorption of simple vacancies. For PZT, however, the situation is more complicated, as can be seen from Figure 1, which shows the atomic structure (schematic only) of a domain wall dislocation in PZT. The position of the wall, which is the glide plane of the dislocation, is shown in Figure 1 as a horizontal dashed line. It is clear that an upward (downward) motion of the domain wall requires that the extra half-plane of the dislocation emit (absorb) $PbO_2$ or $Zr(Ti)O_2$ complexes, which will require higher activation energy than the simply vacancy process. The possibility also exists that the defects involved in climb may be electrically charged, therefore interacting directly with the internal electric field.

The creation of a climb defect is a thermally activated process requiring an energy U. The necessary enthalpy for a unit climb step of a domain wall dislocation is

$$H = U - \tau b^3 \qquad (1)$$

where $\tau b^2$ is the force applied to a length b of dislocation which moves through the same distance b as the climb defect is created; it is assumed in (1) that electrical neutrality is maintained throughout the climb process. The rate of creation of climb defects R in these circumstances is

$$R = \nu \exp\left[-\frac{U - \tau b^3}{kT}\right] \qquad (2)$$

where $\nu$ is the frequency of atomic vibration, k is Boltzmann's constant and T is the absolute temperature.

Assume that the dislocations are spaced a distance $\lambda$ apart, so that the stress is given by

$$\tau = F\frac{\lambda}{b} \tag{3}$$

where F is the uniform pressure tending to move the wall, given in the last report as

$$\frac{F}{\mu} = 1.50\epsilon^2(f-\frac{1}{3}) - 1.56\epsilon^2 f \mp \epsilon\frac{\sigma}{\mu} \tag{4}$$

in which f is the volume fraction of material with c-axis aligned along the poling direction, $\epsilon$ is the misfit and $\sigma$ is the external stress applied normal to the domain wall (positive if tensile). Substituting (4) and (3) into (2), and noting that $\epsilon=\lambda/b$, the velocity of the wall can be expressed as

$$\begin{aligned} v &= \pm\nu b\exp[-\frac{U^*\pm\sigma b^3}{kT}] \\ U^* &= U-\mu b^3\epsilon[1.50\epsilon(f-\frac{1}{3})-1.56\epsilon f] \end{aligned} \tag{5}$$

where the positive (negative) signs apply to tensile (compressive) applied stress. For cyclic stressing, the net migration rate (in cm. per cycle) of the domain wall is

$$\langle v\rangle = 2\nu b\exp[-\frac{U^*}{kT}]\sinh[\frac{\sigma b^3}{kT}] \tag{6}$$

in such a sense as to make the crystal extend along the stress axis. If U is of order 1eV, equation (6) predicts a wall drift of 40$\mu$m in $10^9$ cycles. It is expected that U will be substantially larger, 2eV or more, and in this case the wall motion will be negligible ($10^{22}$ cycles needed for boundary drift of 1nm).

***b. Plans***

⋆ Continued modelling of the mechanisms of ferroelastic domain wall motion will be performed, with the aim of determining critical parameters which can be derived from or compared with experiment. Specific questions to be answered are:

1. Is the wall motion governed by the two-dimensional analog of kink pair nucleation and propagation, or by diffusive dragging of wall defects and dislocations?

2. How are these mechanisms influenced by an electric field of sufficient magnitude to stabilize the poled state?

3. How do the lifetimes of poled and unpoled specimens compare?

*Acta metall. mater.* Vol. 41, No. 2, pp. 643–647, 1993
Printed in Great Britain. 

0956-71[illegible]/93 $6.00 + 0.00


# THE FLOW STRESS OF POTASSIUM

M. S. DUESBERY[1] and Z. S. BASINSKI[2]

[1]Fairfax Materials Research, Inc., 5613 Marble Arch Way, Alexandria, VA 22310-4011, U.S.A. and
[2]Institute for Materials Science, McMaster University Hamilton, Ontario, Canada L8S 4L7

*(Received 18 May 1992)*

**Abstract**—Experimental results on the flow stress of potassium in the temperature range of 1–30 K are compared with atomistic computer simulation of rigid dislocation motion and of dislocation kink pair generation and migration. Quantitative agreement is demonstrated. Implications for the rate theory and the continuum elastic theory of kink pairs are discussed.

## 1. INTRODUCTION

It is now accepted that the large, strongly temperature and orientation dependent flow stress exhibited by even the simplest body-centred cubic (b.c.c.) crystalline materials has its origin in a symmetry-based non-planar structure of the rate-controlling screw dislocation. Suggested first by Hirsch [1], this was established by extensive atomistic simulations which have been reviewed in depth, most recently by Vitek [2] and Duesbery [3].

In the subsequent shift of focus of atomistic simulation to more complex materials, it has been forgotten that some basic but readily addressable questions remain to be answered. To illustrate this more clearly, brief recourse to the history of the subject is in order. During the early 1970s, before the advent of the embedded atom method and its adjuncts [4, 5], the almost universal use of pair potentials led to two distinct approaches. The first of these, acknowledging that the refractory b.c.c. metals cannot be represented with any confidence by pair potentials, concentrated instead on investigating the range of dislocation core properties which could be supported by a b.c.c. lattice bound by empirical pair potentials. This avenue of research was used with great success by Vitek and co-workers [2, 3]. They demonstrated, among other things, the universality of the large Peierls binding energy of the screw dislocation. The second approach, followed by Basinski and colleagues [2, 3], recognised that pair potentials can be used with a high degree of justification for alkali metals and therefore that a combined theoretical and experimental attack on the properties of potassium, the only alkali metal which does not experience a low-temperature martensitic transformation, might permit quantitative agreement to be realised. It is with this second approach that this paper will be concerned.

The work available on potassium is quite extensive. The core structure and mobility of rigid screw dislocations in the presence of shear stresses were investigated theoretically by Basinski *et al.* [6]. This work was extended to encompass general applied stresses by Basinski and Duesbery [7] and by Duesbery [8]. The question of non-rigid screw dislocations was addressed by Duesbery [9], who investigated the structure and mobility of kink pairs in potassium. Meanwhile, the temperature and orientation dependence of the flow stress in potassium for temperatures between 1 and 30 K were measured by Basinski *et al.* [10]. The results of this work were never fully integrated with the original purpose of quantifying computer modelling of the dislocation core. The purpose of this paper to correct this omission. It will be shown that when reliable interatomic forces can be used, a theoretical treatment of the screw dislocation core is sufficient to give a quantitative description of the orientation and temperature dependence of plasticity in a b.c.c. metal. Some associated, fundamental questions will also be discussed.

## 2. THE RIGID SCREW DISLOCATION

The initial work on the mobility of screw dislocations in potassium [6] was performed for rigid, straight dislocations at zero temperature, a restriction common at the time to all core simulations and imposed by computational limitations. Using pure shear strains to apply a force to the core, the Peierls stress was found to lie between $1.05 \times 10^{-2}\,\mu$ ($\mu$ is the $\langle 111\rangle\{hkl\}$ shear modulus) for a strain applied parallel to the *easy* direction on $\{211\}$ planes and $2.2 \times 10^{-2}\,\mu$, for strains applied on $\{110\}$ planes. It was found later [6, 7] that the core in b.c.c. metals is particularly sensitive to the details of the applied stress tensor; calculations for forces applied with uniaxial tensile loading revised the limits on the calculated Peierls stress to between $6.3 \times 10^{-3}\,\mu$ (for $\langle 110\rangle$ loading) and $8.5 \times 10^{-3}\,\mu$ (for loading parallel to an axis in the centre of the standard stereographic triangle).

The experimental work [10], however, showed Peierls stresses varying only from $2.0 \times 10^{-3}\mu$ (for $\langle 110 \rangle$ loads) to $3.3 \times 10^{-4}\mu$ (for centre-triangle loads), even when extrapolated to 0 K. This discrepancy, a factor of 3, is well outside either the experimental error or the theoretical uncertainty and calls into question the validity of the mechanism assumed to be operative in the computer simulations, i.e. the surmounting of the Peierls barrier by a rigid dislocation. At the same time, the experimental measurements of the orientation dependence of the flow stress provided corroborative evidence supporting the simulations. It was found that the flow stress $\tau$, a function of the temperature $T$ and the orientation $\Theta$, could be represented in the separable form

$$\tau(T, \Theta) = f(T) \cdot g(\Theta). \qquad (1)$$

This means that the orientation dependence of the flow stress is an explicit function only of the magnitude of the stress and not of the temperature. In other words, the ratio of the flow stresses for two different orientations at the same temperature is independent of temperature. With the temperature factored out in this way, it was found [10] that the theoretical and experimental orientation dependences of the flow stress in potassium were in close agreement (to within better than $\pm 5\%$). It was shown later [3] that this same reduction (1) could be applied to the experimental measurements of the orientation dependence of the flow stress in refractory b.c.c. metals with considerable success (standard deviations reduced in all cases but one to better than 10% from up to 30%).

The picture presented at this stage was of a modelling procedure which agreed well with experiment in one respect, the orientation dependence of the Peierls stress, but which was sadly lacking in its prediction of the magnitude and temperature dependence of the Peierls stress.

## 3. KINK PAIRS AND THERMAL ACTIVATION

The generation and propagation of kink pairs in potassium were modelled by Duesbery [9], using a model containing $10^5$ atoms arranged in a block of dimensions $30b \times 30b$ ($b$ is the magnitude of the Burgers vector) normal to the dislocation line and $150b$ parallel to the dislocation line. In what was strictly a zero temperature calculation, kink pairs of varying separation were equilibriated with respect to an applied stress of such a sense as to expand the pairs. From this stress–separation data it is possible to extract the thermodynamic parameters which appear in the standard Arrhenius expression for the strain rate $\dot{\epsilon}$

$$\dot{\epsilon} = \dot{\epsilon}_0 c^{-H/kT} = \dot{\epsilon}_0 e^{-\frac{(E(\tau) - \tau b A)}{kT}} \qquad (2)$$

in which $k$ is Boltzmann's constant, $T$ is the temperature and $\dot{\epsilon}_0$ a pre-exponential factor to be discussed below. As indicated in (2), the activation enthalpy $H$ for a kink pair in the presence of an applied stress $\tau$

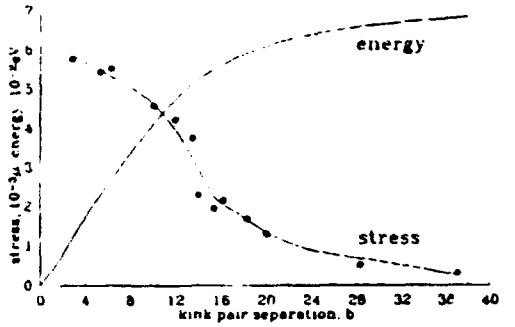


Fig. 1. The equilibrium stress and configurational energy of a kink pair complex in potassium as a function of kink separation.

consists of two parts. The first is the configurational energy $E(\tau)$ of the complex. This term is reduced by the external work done, which is the product of the applied stress $\tau$, the area $A$ swept by the activation process and the displacement $b$ through which the area is translated.

The stress–separation data obtained earlier [9] are reproduced in Fig. 1. The scatter in the data points is larger than is usual for theoretical work. This is indicative of the difficulty of the calculations. The equilibrium states are unstable, so that the isolation of their location requires the application of a trial bias stress together with a superimposed oscillating stress of steadily decreasing amplitude. The curve drawn through the data points is a least squares spline fit. For small separations, the stress is nearly constant. In this regime, as discussed earlier [9], the kink pair is simply a bulge in the dislocation line, with height less than the distance between two Peierls valleys. The height and width of the bulge increase in constant proportion until the adjacent Peierls minimum is reached. The kinks then separate according to classical expectations with consequent decrease in stress. The energy curve in Fig. 1 was obtained by integration of the stress–separation curve; the energy values are slightly higher than those reported previously [9], but are more accurate, in good agreement with the asymptotic limit of twice the energy of an isolated kink, calculated from a model containing only a single kink to be 0.038 eV [9].

The information in Fig. 1 can be reprocessed to give the activation enthalpy as a function of stress. The energy $E(\tau)$ is taken directly from the relevant curve and the swept area $A$ is estimated by multiplying the kink pair separation by the kink height $a$. This latter procedure is not accurate for large stresses, when the kink pair height does not reach its full extent, but this does not affect the arguments which follow. The result is shown in Fig. 2. The enthalpy drops from a high of 0.076 eV at zero stress [when the work term in (2) is identically zero] to 0 for a kink pair separation of about $12b$, corresponding to a stress of $4 \times 10^{-3}\mu$ (at this stress level the use of the full kink height in the area calculation is accurate).

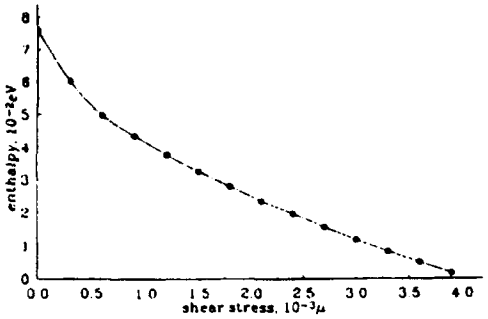


Fig. 2. Logarithmic plot of stress against kink pair separation.

This stress in only half that required to move a rigid dislocation of 0 K and leads to the conclusion, contrary to conventional expectation, that the motion of rigid dislocations may be superseded even at the lowest temperatures by kink pair activation.

The experimental work [10] indicates that the activation enthalpy is closely proportional to the temperature for temperatures below 20 K, with a slope of $20k$. Using this single piece of empirical information to fix a value for the ratio $\dot{\epsilon}/\dot{\epsilon}_0$ in (2), the theoretical temperature dependence of the flow stress $\tau$ can be estimated from the data in Fig. 2. The results are shown in Fig. 3, together with the experimental measurements from [10], each normalised to the flow stress at 4.2 K. Agreement is satisfactory up to 20 K. Above this temperature the comparison is invalid, because the experimental proportionality between $H$ and $T$ breaks down. There remains a small discrepancy between the absolute values of the experimental and theoretical flow stresses. For an orientation corresponding to the constraint used in the kink modelling work [9] (a pure shear strain acting on $\langle 111\rangle\{110\}$), the experimental values at 4.2 K range from 2.8 to $3.3 \times 10^{-3}\,\mu$. The theoretical estimate is $3.9 \times 10^{-3}\,\mu$, about 20% too high. Nevertheless, the overall agreement demonstrates that computer simulation methods can give quantitative results for structures in which the interatomic forces can be reliably approximated.

An obvious question arises as to why the rigid dislocation core calculations were found adequate for calculation of the orientation dependence of the flow stress. In the absence of definitive kink pair calculations as a function of general applied stresses, this remains a matter of informed conjecture. The mobility of the rigid dislocation depends strongly on the shape of the core, which depends in turn on the detailed nature of the applied stress. In other words, the magnitude of the Peierls potential depends critically on the external stress. Since the energy of the kink pair complex also depends on the Peierls potential, it is not unreasonable to suppose that the rigid dislocation orientation dependence carries through to kink pair activation.

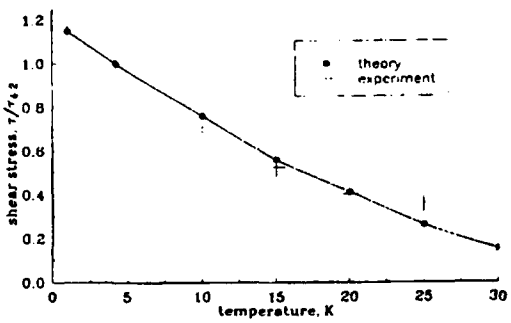


Fig. 3. The normalised theoretical and experimental temperature dependence of the flow stress in potassium.

## 4. CRITICAL QUANTITIES

The calculations reported in the previous section are self-consistent, independent of both elasticity theory and experiment, except for the use of the experimentally observed value and constancy of the exponent $H/kT$. The results can therefore be used with some degree of confidence to examine some associated, critical questions and quantities.

First to be considered will be the pre-exponential factor $\dot{\epsilon}_0$, which can be decomposed according to standard rate theory into

$$\dot{\epsilon}_0 = \frac{\rho}{\lambda}\,\Lambda a b \nu(\lambda) \tag{3}$$

where $\rho$ is the dislocation density, $a$ is the kink pair height, $\nu(\lambda)$ is the attack frequency at the critical activation length $\lambda$ and $\Lambda$ is the kink mean free path. As noted above, experiment indicates a value for $\ln(\dot{\epsilon}/\dot{\epsilon}_0)$ of 20. The question is whether or not this number is consistent with reasonable magnitudes for the physical quantities involved. The experiments [10] were performed for a tensile strain rate of $3.4 \times 10^{-4}\,\mathrm{s}^{-1}$. Taking half this value as the shear strain rate, a value of $8.25 \times 10^{4}$ is obtained for $\dot{\epsilon}_0$. Using a value of 0.3 THz for the frequency of transverse phonons with wave vector parallel to $\langle 111\rangle$ and wavelength of $25b$ ($\lambda \approx 12.5b$) in potassium [11] and setting $a \approx b = 0.475$ nm, consistency requires the product $\rho\Lambda$ to have a value of $1.44 \times 10^{4}\,\mathrm{m}^{-1}$. With a reasonable mobile dislocation density at yield of $10^{11}\,\mathrm{m}^{-2}$, the kink mean free path must be $300b$, an acceptable value. Participation of vibrational modes with larger wavelength (the 0.3 THz mode, with $h\nu \approx 2.6\,kT$ at 4 K, is partially quenched) would reduce this predicted mean free path.

The second critical quantity to be considered concerns the elastic interaction of kinks, the continuum elastic theory of which indicates that the two members of a kink pair of height $a$ and separation $l$ attract each other with a force given by [12]

$$F = \frac{a^2 b^2}{2l^2}\left[W(\theta) + \frac{\partial^2 W(\theta)}{\partial\theta^2}\right] \tag{4}$$

where $W(\theta)$ is the anisotropic elastic energy factor of a dislocation line of character angle $\theta$ (i.e. such that

the energy per unit length of the dislocation line is $W(\theta)b^2 \ln(R/\rho)$, where $R$ and $\rho$ are outer and inner radii). The expression (4) is valid provided that the kink separation is much larger than the kink width. While this is not true in the present case, since the maximum pair separation is only about four times the kink width, it might be expected that (4) would be a fair approximation. A more important drawback of (4) is the assumption that standard linear elasticity can be applied to dislocation segments with length of the same order as the inner cutoff radius. For b.c.c. metals, in which the screw dislocation core is known to be highly structured over distances of this order and in which the kinks pass over a Peierls energy barrier, this assumption is in particular doubt.

There is sufficient information in the data outlined above to test the applicability of (4). In the saddle point state, the force (4) can be equated to the force $\tau ab$ exerted on a kink by the applied stress. The resulting formula relates the stress directly to the kink pair separation and can be tested using the data from Fig. 1. The results are shown in Fig. 4. The straight line, drawn to have a slope of $-2$ and positioned by eye, shows that the inverse square law of (4) is obeyed well for stresses less than $4.5 \times 10^{-3}\mu$. It was reported incorrectly [9], as pointed out by Kirchner [13], that the intercept of this line was also compatible with (4). In fact, this is not the case at all. The intercept of the line at $\ln \tau = 0$ occurs at $l = 22.9b$. Since the kinks are very wide, it is reasonable to assign to them the stiffness of a screw dislocation, that is, $[W(0) + W''(0)] = 5.3$ GPa. Using these quantities with the value of $\mu = 1.3$ GPa in (4), an effective kink height of $a = 2.6b$ is obtained.

This source of this discrepancy could lie in an insufficiency of the expression (4) or in the assumption that the force on a kink is $\tau ba$. The latter is unlikely, since it is based on thermodynamic arguments. It must be concluded that the elastic force acting between two kinks in the b.c.c. structure is of the same functional form as (4), but of substantially larger magnitude. Interesting in this respect is a recent suggestion by Seeger [14]. In analyses of the temperature dependence of the flow stress in refractory metals in terms of the kink pair mechanism, using (4), values of $a = 1.5b$ to $1.8b$ were obtained for the kink height. From this deduction it was concluded that the predominant kink in b.c.c. metals was the *double kink*, extending over two Peierls hills. Calculations using both pair and embedded atom potentials [3] do not support this conclusion. In the light of the present results, it seems more likely that the deduced extent of the *double kink* is a manifestation of the breakdown of the elastic expression (4).

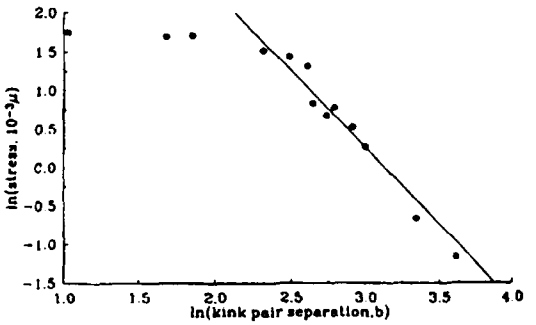


Fig. 4. The activation enthalpy for kink pairs in potassium as a function of applied stress.

## 5. SUMMARY AND CONCLUSIONS

The results described above show that quantitative predictions can be made with the use of atomistic computer modelling methods when the interatomic forces are known with some precision. It would be an interesting exercise to determine whether the modern embedded atom potentials can provide a similarly satisfactory description of the refractory b.c.c. and other transition metals. In view of the results presented above, this might be considered a critical test of the reliability of the potentials for use in calculation of other properties.

The low-temperature deformation of potassium has been shown to be governed by the generation of fully formed kink pairs. The mutual interaction of the kinks which form the pair was found to have the same functional dependence on separation as is predicted by classical elasticity, but a magnitude larger by more than a factor of 2. The discrepancy is tentatively attributed to one or more of several factors, including the application of the line tension model of a dislocation to kinks with a Peierls energy and to the atomic dimensions and commensuracy of the kink height and the dislocation core structure. Further work is needed to resolve this problem. Particularly illuminating would be the properties of a system controlled by incomplete kink pair generation (i.e. in the high-stress regime when the height of the critical kink complex is less than a repeat spacing) and of a system controlled by kink migration rather than generation. Both types of system are likely to be encountered with refractory b.c.c. metals and with semiconductors [3].

Most computer simulation work, to this day, is confined to consideration of straight, rigid dislocations. This constraint, no longer imposed by computational capability, is difficult to justify in the light of modern knowledge that, with few exceptions, dislocations move by kink pair activation and migration. There is no doubt that the study of rigid dislocations can provide much useful information in return for limited effort. For example, the orientation dependence of dislocation mobility can be assessed with some confidence. However, bridging the gap between the atomistic and macroscopic scales by means of linear elasticity can be a dangerous procedure, as shown above. Larger scale, three-dimensional atomistic calculations are needed to establish a reliable continuum interface.

*Acknowledgement*—Part of this research was sponsored by the Office of Naval Research under contract N00014-91-C-0067.

## REFERENCES

1. P. B. Hirsch, *Proc. 5th. Int. Conf. on Crystallography*, Cambridge, oral communication, p. 139 (1960).
2. V. Vitek, *Proc. Int. Symp. Dislocations and Properties of Real Materials*, p. 30. Physical Society, London (1985).
3. M. S. Duesbery, *Dislocations in Solids* (edited by F. R. N. Nabarro), Vol. 8, p. 67. North-Holland, New York (1989); M. S. Duesbery and G. Y. Richardson, *CRC Cri. Rev. solid St. Mater. Sci.* **17**, 1 (1991).
4. M. S. Daw and M. I. Baskes, *Phys. Rev. B* **29**, 6443 (1984).
5. M. W. Finnis and J. E. Sinclair, *Phil. Mag. A* **50**, 45 (1984).
6. Z. S. Basinski, M. S. Duesbery and R. Taylor, *Can. J. Phys.* **48**, 1480 (1970).
7. Z. S. Basinski and M. S. Duesbery, *Proc. Int. Conf. Dislocation Modelling of Physical Systems* (edited by M. F. Ashby, R. Bullough, C. S. Hartley and J. P. Hirth), p. 273. Pergamon Press, New York (1981).
8. M. S. Duesbery, *Proc. R. Soc. Lond. A* **392**, 145, 175 (1984).
9. M. S. Duesbery, *Acta metall.* **31**, 1747, 1759 (1983).
10. Z. S. Basinski, M. S. Duesbery and G. S. Murthy, *Acta metall.* **29**, 801 (1981).
11. W. J. L. Buyers and R. A. Cowley, *Phys. Rev.* **180**, 755 (1969).
12. J. P. Hirth and J. Lothe, *Theory of Dislocations*, 2nd edn, p. 245. Wiley, New York (1982).
13. H. O. K. Kirchner, private communication (1984).
14. A. Seeger, *Proc. Int. Conf. Dislocations*, p. 141. CNRS (1984).

# Self-Repair of Monolayers with Vacancy Damage

B. Joós[a]

*Ottawa Carleton Institute of Physics, University of Ottawa Campus, Ottawa, Ontario, Canada K1N-6N5*

M. S. Duesbery[b]

*Fairfax Materials Research Inc., 5613 Marble Arch Way, Alexandria, Virginia 22310-4011*

(Received 19 October 1992)

Lennard-Jones monolayers are shown by molecular dynamics simulation to exhibit a self-healing behavior which involves a rapid condensation of vacancies into dislocation dipoles. An associated collapse of the shear modulus similar to the Kosterlitz-Thouless dipole dissociation occurs for high vacancy concentrations. By contrast monolayers having nearest neighbor piecewise linear interactions are found to cavitate by agglomeration of vacancies into clusters.

PACS numbers: 62.20.Dc, 61.72.Ji, 68.55.Ln

Vacancy damage is a common occurrence in monolayers and thin films, more so than in bulk solids because thermodynamic equilibrium in the former involves exchange with the external environment as well as entropic considerations. Vacancies are particularly abundant in physisorbed monolayers, in which the concentration can be as high as 10% before the melting point is reached [1]. This Letter shows that, although vacancies are local defects, a concentration of just a few percent can have profound consequences on the macroscopic physical properties of a monolayer. Specifically we demonstrate, by molecular dynamics simulation, a unique self-repair mechanism which leads to a shear modulus collapse similar to the melting scenario proposed in the Kosterlitz-Thouless-Halperin-Nelson-Young (KTHNY) [2] theory of two-dimensional melting. In this new mechanism, vacancies condense rapidly into dislocation dipoles, repairing the lattice; the dipoles then dissociate inducing a quasifluid state. These effects occur for temperatures just above the self-diffusion temperature.

Monolayers can appear in many forms with various interactions. We focus on monolayers formed of atoms interacting with spherical potentials. Two potentials are considered, one long range, the Lennard-Jones potential (LJP), and the other short range, the nearest neighbor piecewise parabolic potential (PWPP). The effects discussed above are seen in the LJP monolayer. The other system, the PWPP monolayer, exhibits very different behavior. It does not heal but develops voids.

The LJP energy between two atoms at a distance $r$ from each other is given by

$$V_{LJ}(r)=4\epsilon\left[\left(\frac{\sigma}{r}\right)^{12}-\left(\frac{\sigma}{r}\right)^{6}\right]. \tag{1}$$

The PWPP energy between two atoms at a distance $r$ from each other is given by

$$V_{PWP}(r)=\begin{cases}\frac{1}{2}\kappa(r-d_0)^2-\kappa w^2, & r\le d_0+w,\\ -\frac{1}{2}\kappa(r-d_0-2w)^2, & d_0+w<r\le d_0+2w,\\ 0, & r>d_0+2w.\end{cases} \tag{2}$$

$w$ is taken to be $0.15d_0$ as in Ref. [3]. For this value of $w$ the dislocation core has only one broken bond. Larger values of $w$ lead to more broken bonds in the core [4].

Monolayers formed of particles interacting with these potentials condense into triangular lattices. Both types of monolayers have been extensively studied although the motivations of the studies were different. The PWPP has been used mostly in simulations of the plasticity of solids [3,4] whereas the LJP was used extensively in attempts to understand the nature of the melting transition in two dimensions (for reviews see Refs. [5] and [6]). Recently the melting behavior of the PWPP was also considered [7].

An expression for the elastic constants, which is valid at finite temperatures, can be derived by noticing that the elastic constants are the second derivatives of the Helmholtz free energy, $\Omega=-kT\ln Z$, with respect to the various Lagrange strains $\eta_{ij}$ [8]:

$$C_{ijpq}=\frac{1}{A}\left(\frac{\partial^2\Omega}{\partial\eta_{ij}\partial\eta_{pq}}\right). \tag{3}$$

The classical partition function $Z$ for the crystal is a relatively simple sum over all configurational energies.

For an isotropic solid such as the two-dimensional triangular lattice, there are only two independent elastic constants. Traditionally the following two are chosen to characterize the system:

$$C_{1122}=C_{12}=\lambda=\frac{1}{AkT}\left\{\left\langle\sum\frac{\phi'}{r}(\Delta x)^2\right\rangle\left\langle\sum\frac{\phi'}{r}(\Delta y)^2\right\rangle-\left\langle\sum\frac{\phi'}{r}(\Delta x)^2\otimes\sum\frac{\phi'}{r}(\Delta y)^2\right\rangle\right\}$$
$$+\frac{1}{A}\left\langle\sum\frac{\phi''}{r^2}(\Delta x)^2(\Delta y)^2\right\rangle-\frac{1}{A}\left\langle\sum\frac{\phi'}{r^3}(\Delta x)^2(\Delta y)^2\right\rangle+\frac{1}{A}\left\langle\sum\frac{\phi'}{r}(\Delta x)^2\right\rangle, \tag{4}$$

$$C_{1212}=C_{44}=\mu=\frac{1}{AkT}\left\{\left\langle\sum\frac{\phi'}{r}\Delta x\Delta y\right\rangle^2-\left\langle\left[\sum\frac{\phi'}{r}\Delta x\Delta y\right]^2\right\rangle\right\}$$
$$+\frac{1}{A}\left\langle\sum\frac{\phi''}{r^2}(\Delta x)^2(\Delta y)^2\right\rangle-\frac{1}{A}\left\langle\sum\frac{\phi'}{r^3}(\Delta x)^2(\Delta y)^2\right\rangle+\frac{NkT}{A}, \quad (5$$

where the quantities $\Delta x$ and $\Delta y$ represent the $x$ and $y$ coordinates of $(x^{\alpha l}-x^{\alpha' l'})$, $r$ the modulus of that vector, and $A$ the area of the system. The terms in braces are referred to as the "fluctuation terms" while the following terms in each expression constitute the "Born terms." The last term in Eq. (5) is the kinetic energy contribution.

For canonical ensembles the above equations [(4) and (5)] are equivalent to the ones given by Ray, Moody, and Rahman [9]. Whether the molecular dynamics simulation is done at constant pressure or constant volume, the sums on the particle momenta can be factored out using the equipartition theorem. This is the case provided the simulation maintains a canonical ensemble.

To simulate a physically realistic system we have performed simulations at constant pressure and varied the temperature. A slightly compressed monolayer was chosen. The two potentials have been chosen to have the same depth ($\epsilon=\kappa w^2$) and the same minimum ($\sigma=2^{-1/6}d_0$).

The zero temperature elastic constants for a perfect lattice at a pressure of $0.0053\kappa$ with the LJP interaction are $\lambda=0.836\kappa$ and $\mu=0.825\kappa$ whereas with the PWPP they are $\lambda=0.440\kappa$ and $\mu=0.429\kappa$. The LJP system is a stiffer solid.

Figure 1 shows the variation, as a function of vacancy concentration $c_n$, of the shear modulus ($\mu$) and the bulk modulus ($B=\lambda+\mu$), normalized to their respective perfect lattice values $\mu_0$ and $B_0$. Vacancy concentrations from 0 to 3.8 at.% were considered and the calculations were done at a low temperature, $0.002\kappa d_0^2/k$, where $k$ is the Boltzmann factor. (N.B. The melting temperature for both systems is about $0.011\kappa d_0^2/k$.)

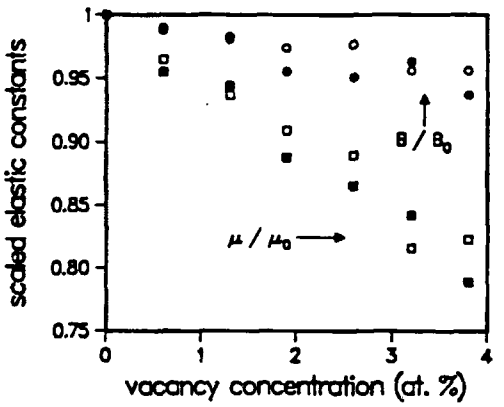


FIG. 1. Variation of the shear modulus $\mu$ (squares) and the bulk modulus $B=\lambda+\mu$ (circles), both normalized to the zero vacancy values $\mu_0$ and $B_0$, respectively, as a function of vacancy concentration for the LJP (full symbols) and PWPP (open symbols) systems at the temperature $0.002\kappa d_0^2/k_B$.

The range of the potential seems to have little effect on the rate of decrease of the shear modulus with increasing vacancy concentration. The shear modulus loses a fifth of its value for a 4 at.% concentration of vacancies. This corresponds to $\Delta\mu/\mu_0=(\mu-\mu_0)/\mu_0=-5c_n$. The bulk modulus on the other hand is less sensitive to vacancy defects; the rate of decrease is considerably smaller ($\Delta B/B_0\simeq-1.25c_n$). As Fig. 1 shows, there is a scatter in the data with vacancies present. For each concentration there are many possible configurations of vacancies. Figure 1 shows one configuration for each studied concentration.

As the temperature is raised, the vacancies start to move. In both systems the self-diffusion temperature for vacancies is approximately $0.0055\pm0.0005\kappa d_0^2/k$. The two systems, however, show rather different behavior.

In the LJP system, the vacancies, when in sufficient number, condense into a dislocation dipole. The sample in our simulations is a rhombus with 28 atoms on the side. Periodic boundary conditions are used. For fewer than 15 vacancies (or $c_n<1.9\%$) the vacancies diffu into small vacancy clusters. For 15 vacancies or more (or $c_n\geq1.9\%$) the vacancies are removed by condensing into a "large" vacancy dislocation dipole (separation equal to or larger than 15 atomic rows) [see Fig. 2(b)] [10,11]. The periodic boundary conditions introduce a periodicity in the behavior of our system [see Fig. 3(a)]. For more than 28 vacancies (or $c_n>3.6\%$) there are more vacancies than would fit into one dipole, so 28 vacancies are annealed out and the remainder form vacancy clusters unless their numbers exceed the minimum required to form a second "large" dipole. When a dipole is present in the sample, the shear modulus collapses [see Fig. 3(a)]. It takes about a time of $30000t_0$ to form a "large" dipole, i.e., about 20 ns if parameters appropriate to Xe are used ($t_0$ is the unit of time $\sqrt{m/\kappa}$). This is an upper limit obtained with vacancies uniformly placed on the sample. With other configurations the times were shorter. Modulations in a substrate holding field could, however, make these times much longer, leading to an increase in the concentration of vacancies (e.g., Xe monolayers adsorbed on graphite [1]).

The above results are in accord with our findings on the properties of dislocation dipoles [10–12]. In these references it is shown that dipoles containing fewer than 15 vacancies behave more like composite pinned defects tha elastic dipoles. They are the favored defects at very lo vacancy concentrations. On the other hand a logarithmic dependence of the energy on size makes large dipoles

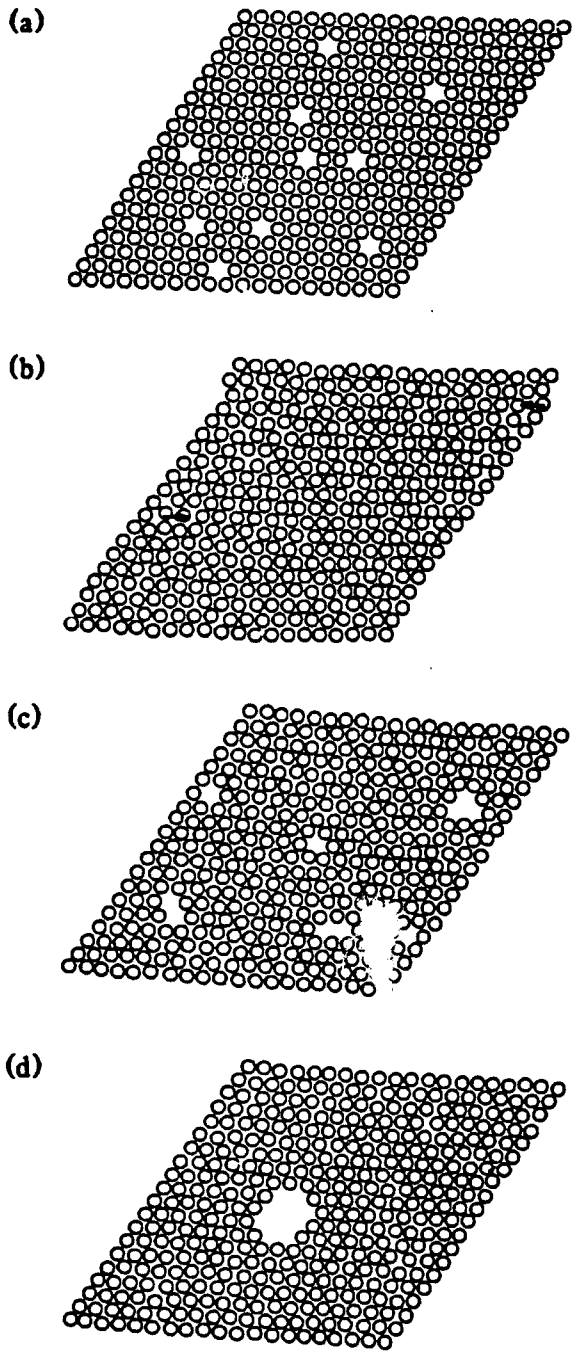


FIG. 2. (a) Typical low temperature configuration of atoms for either the LJP or PWPP system for a vacancy concentration of $c_v = 2.5$ at.%. (b) Same configuration after relaxation with the LJP interaction at the temperature $T = 0.006\kappa d_0^2/k_B$. (c),(d) Same as (b) but with the PWPP interaction; (c) is an intermediate configuration and (d) the final configuration.

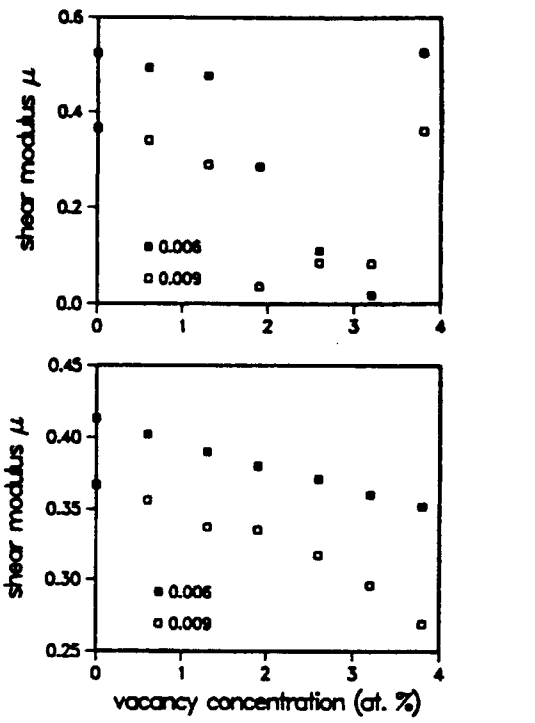


FIG. 3. Variation of the shear modulus as a function of vacancy concentration for temperatures of 0.006 and $0.009\kappa d_0^2/k_B$ for (a) the LJP system (at a pressure $P = 0.0087\kappa$) and (b) the PWPP system ($P = 0.0053\kappa$).

favorable at higher concentrations. These move nearly freely in the direction of their Burgers vector over a wide range of angles (45° to 135°) [12] and are easily screened out by similar dipoles (in our case in the neighboring cells of our periodic structure). When present they lead to the loss of shear strength and translational order.

When particles interact with the short-range PWPP, the vacancies form clusters which eventually combine into large voids [see Figs. 2(c) and 2(d)]. This typically takes much longer than the condensation in the LJP system because of the short range of the interaction (1 to 2 orders of magnitude longer). The PWPP is nearest neighbor, so as soon as a triangle of vacancies is formed, additional vacancies in the cluster do not add to the energy. In effect, one has a free surface, and the vacancies anneal out but remain within the system. The temperature-induced diffusion smooths out the elastic constants even before the voids are formed [see Fig. 3(b)]. There is no collapse of the shear modulus, which is reduced only by an amount comparable to the reduction in density.

In summary, just above the self-diffusion temperature and well below the melting temperature, only a very low concentration of isolated vacancies can be sustained in a monolayer. What happens to the vacancies depends strongly on the range of the interparticle interaction. A short-range interaction favors cavitation. Monolayers with long-range interparticle interactions permit the healing of the monolayer, leaving behind a dislocation dipole and a disordered state. The speed of this healing is remarkable, of the order of nanoseconds when rare gas parameters are used.

The latter mechanism may be applicable to the melting of some physisorbed monolayers, in particular those with a weak substrate corrugation, such as Xe on Ag{111}. In an experimental environment thermal vacancies are unavoidable. They may permit a melting transition involving the creation of dislocation dipoles and their dissociation, a process proposed by KTHNY [2] and which some experiments support. Existing simulations ignore ingrown vacancies and do not see such a mechanism [5,6].

The authors wish to thank D. G. Rancourt for a critical reading of the manuscript. This work has been supported by the Natural Sciences and Engineering Research Council of Canada and the Office of Naval Research under Contract No. N00014-91-C-0067.

---

[a]Electronic address: BJOSJ@ACADVM1.UOTTAWA.CA

[b]Electronic address: DUESBERY@NRL.NAVY.MIL

[1] R. J. Birgeneau (private communication).

[2] J. M. Kosterlitz and D. J. Thouless, J. Phys. C **6**, 1181 (1973); D. R. Nelson and B. I. Halperin, Phys. Rev. B **19**, 2457 (1979); A. P. Young, Phys. Rev. B **19**, 1855 (1979).

[3] A. J. C. Ladd and W. G. Hoover, Phys. Rev. B **26**, 5469 (1982).

[4] W. G. Hoover, N. E. Hoover, and W. C. Moss, J. Ar Phys. **50**, 829 (1979); W. G. Hoover, W. T. Ashurst, a... R. J. Olness, J. Chem. Phys. **60**, 4043 (1974); A. J. C. Ladd and W. G. Hoover, J. Chem. Phys. **74**, 1337 (1981); W. G. Hoover, A. J. C. Ladd, and N. E. Hoover, in *Interatomic Potentials and Crystalline Defects*, edited by J. K. Lee (Metallurgical Society, Warrendale, PA, 1981).

[5] F. F. Abraham, Adv. Phys. **35**, 1 (1986).

[6] K. Strandburg, Rev. Mod. Phys. **60**, 161 (1988).

[7] J. A. Combs, Phys. Rev. Lett. **61**, 714 (1988); Phys. Rev. B **38**, 6751 (1988).

[8] D. R. Squire, A. C. Holt, and W. G. Hoover, Physica (Utrecht) **42**, 388 (1969).

[9] J. R. Ray, M. C. Moody, and A. Rahman, Phys. Rev. B **32**, 733 (1985).

[10] M. S. Duesbery and B. Joós, Philos. Mag. A **54**, 145 (1985) (in Fig. 1 the labels for $\lambda$ and $\mu$ have been inverted).

[11] B. Joós and M. S. Duesbery, Phys. Rev. Lett. **55**, 1997 (1985); Phys. Rev. B **33**, 8632 (1986).

[12] B. Grossmann, B. Joós, and M. S. Duesbery, Phys. Rev. B **39**, 7917 (1989); B. Joós, Q. Ren, and M. S. Duesbery (to be published).

accepted into Philos. Mag.

# On Hardening by Dispersed Spherical Particles

N.P. Louat and M.S. Duesbery

Fairfax Materials Research
5613 Marble Arch Way
Alexandria, VA 22310-4011

Abstract: The methods of Boltzmann's classical statistical mechanics have been used to calculate the hardening at 0K due to a random dispersion of spherical particles with finite size.

## Introduction

Previous analytic methods for treatment of dispersion hardening have been confined to point (i.e. dimensionless) obstacles. In the work described here, these methods are extended to deal with the case where the particles are of finite size, spherical and of radius r.

We seek to determine the yield strength at 0K of a material hardened by the presence of spherical particles which act as simple

blocks to the motion of dislocations. The analysis is based on a consideration of the stability of a sequence of lengths of a single dislocation which has impinged on spherical particles while traversing a slip plane.

Analysis

We assume:

that when acted on by a uniform stress $\sigma$, dislocations with Burgers vector b are bent into arcs of circles of radius R,

$$R=\frac{\mu b}{\sigma} \qquad (1)$$

where $\mu$ is the shear modulus of the deforming material;

that impenetrable particles are randomly distributed and are of strength F which can be expressed in terms of the dislocation line tension ~ $\mu b^2/2$ and the breaking angle $\alpha(a)$ (a is the radius of the circle of intersection between particle and slip plane) by

$$F = \mu b^2 \sin \alpha(a)$$

where each breaking angle ($\alpha$) relates to an individual particle, being, in particular, a function of the radius, a, of the circle of intersection of the operative slip plane with the particle, and;

that the yield stress is the largest stress for which it is possible to have a stable dislocation join an infinite number of particles along a line which is essentially straight and hence does

not cross itself.

Towards the determination of this stress we shall use the theoretical analysis first introduced by Hanson and Morris [1] and subsequently modified and employed by Labusch [2] and by Louat (3) to determine the yield strength due to a dispersion of point obstacles characterized by the same maximum restraining force:

$$F \sim \mu b^2 \sin\alpha_m \sim \alpha_m \mu b^2. \qquad (2)$$

In this case the breaking angle $\alpha$ is the same for all obstacles.

This analysis rested on the rolling circle technique employed by Foreman and Makin [4] in their numerical investigation of this hardening. Thus, it was argued (see fig. 1a) that a dislocation stable at a sequence of positions - - -,k-2, k-1, would also be stable at the next position k provided the particle associated with the k+1$^{th}$ position was centered anywhere in the region, as shown hatched (fig. 1b), traversed by a rolling circle; this region is bounded by an angle $\theta \leq 2\alpha$. Further, for a concentration of obstacles, c, the probability that the point, k, lies in a particular area $\Delta A$ of A is

$$1-e^{-c\,\delta A} \sim c\delta A,$$

provided c $\delta$A is sufficiently small.

Fig. 1a. Rolling circle

Fig. 1.b. Relationship between

sweeping area A. $t_k$ and $\phi$.

In order that such a sequence of lengths represent a dislocation line it is necessary that they not cross themselves.

Here, we shall adapt the treatment of Hanson and Morris [1] to the case where the strength of a particular obstacle depends on the radius of the circle of intersection between the spherical particle concerned and the slip plane. To proceed, we note first from fig. (1 a.), in the case of point obstacles that, following the path of a rolling circle, the angle turned between successive tangents, $t_k$, is equal to the angle, $\phi$, which gives the direction of the trailing circle edge at the point of rotation (see fig (1 b)). It is then readily seen that in the case of an obstacle with radius , a, the angle turned becomes:

$$\overline{\phi} = \phi \left( 1 + a / R \right) \equiv T \phi,$$

where R is as defined in (1).

Then, if the number of points be N and if the angle $\phi$ occurs $n_i$ (i = 1,n) times we have:

$$N = \sum_{i=1}^{n} n_i \qquad (3)$$

and the total angle turned is

$$\sum_{i=1}^{n} n_i \overline{\phi_i} = \Phi \qquad (4)$$

If N is indefinitely large, but $\Phi$ finite, the average value of $\phi_i$ is zero. In this case the whole dislocation line is either straight or contains equal numbers of complete clockwise and anticlockwise rotations. The latter configurations are situations of low

probability which we can neglect.

The procedure for the determination of the thermodynamic probability is akin to that employed to determine the Maxwell-Boltzmann distribution of kinetic energies in an ideal monatomic gas. Thus, if there are n partitions at each of N points the thermodynamic probability that the $i^{th}$ region is occupied $n_i$ times is:

$$P = \frac{(N\,!)\prod_{i=1}^{n} p_i^{n_i}}{\prod_{i=1}^{n} n\,!}, \qquad (5)$$

where $p_i$ is the occupational probability of the $i^{th}$ region . To determine $p_i$ we divide the swept area, A, of fig.(1b) into n regions of area, $\Delta A_i$ (i = 1,n) each characterized by a value of $\phi$, say $\phi_i$ and see that when the concentration of second phase particles is C and provided the area $\Delta A_i$ is sufficiently small, the probability that a point k lies in a particular area $\Delta A_i$ is:

$$p_i \equiv 1-e^{-C\Delta A_i} = 1-e^{\frac{-3\,\pi\, f\,\Delta A_i}{2\,\pi\, r^2}} \sim C\Delta A_i \qquad (6)$$

Here, we have expressed C in terms of the volume fraction, f, of second phase. Thus, we have allowed that the number, M, of particles per unit volume is such that

$$\frac{4\pi r^3 M}{3} = f,$$

where f is the volume fraction of the dispersed phase. It then follows that the concentration, C, of circles of intersection of particles by a slip plane is:

$$C=2r\,M=\frac{3f}{2\pi r^2}.$$

On the basis that the most probable configuration of a system having a large number of parts, is that which actually occurs, we see that to determine this configuration, we have only to maximize it probability, P, subject to the constraints offered by (3) and(4). To proceed, we take advantage of the facts that N and $n_i$ are both large and employ Stirling's approximation for the factorials in (5) and then set the variation in ln P to zero. We find:

$$\delta \ln p = \sum_{i=1}^{n} \delta n_i + \ln p_I - \sum_{i=1}^{n} \ln n_i$$

while (3) and(4) become:

$$\sum_{i=1}^{n} \delta n_i = 0, \qquad (7)$$

$$\sum_{i=1}^{n} \delta n_i \overline{\phi_i} = 0. \qquad (8)$$

Whence introducing the Lagrangian multipliers $\lambda$ and $\gamma$ we have

$$\ln p_i - \ln n_i + \gamma + \lambda\overline{\phi_i} = 0$$

so that, using (3)

$$n_i = \frac{N p_i e^{\lambda\phi_i}}{\sum_{i=1}^{n} p_i e^{\lambda \phi_i}}, \qquad (9)$$

Then from (4) we have

Then, on substituting for $n_i$ in the logarithm of P and after some manipulation we find that:

$$N\sum_{i=1}^{n} e^{\lambda\phi_i}\,\phi_i\,p_i = \Phi\,S,$$

*where*

$$\sum_{i=1}^{n}\phi_i e^{\lambda\phi_i} = S. \qquad (10)$$

$$P = S^N e^{-\lambda\phi} \qquad (11)$$

Invoking (6) and (9) and proceeding to the limit of small quantities $\delta A_i$ , (11) becomes:

$$P = e^{-\lambda\phi}\,[c\int e^{\lambda\phi} dA]^N.$$

We have now to determine S and $\lambda$ . Here, where integration is over the area, A, indicated in fig.(1a) we have, for a/2R<<1:

$$S = C\int_0^{2R} (1+r)\,dl \int_{T(\arcsin l/2R)}^{T(2\alpha-\arcsin l/2R)} e^{\lambda\phi} d\phi$$

$$\sim \frac{C\,R^2 T\,(e^{2\alpha\lambda T}-1)}{\lambda}\,\frac{(1+e^{-\pi\lambda T})}{(\lambda T)^2+1} \qquad (12)$$

The determination of $\lambda$ is assisted by the realization that

$$\frac{d\,\ln S}{d\lambda} = \frac{1}{S}\,\frac{dS}{d\lambda} = \sum_{i=1}^{n}\frac{\phi_i e^{\lambda\phi_i} p_i}{S} = \frac{\Phi}{N} \to 0 \text{ as } N \to \infty \qquad (13)$$

and that $\lambda$ must be such that

$$\frac{dS}{d\lambda} = 0.$$

Nevertheless, this question can only be resolved numerically. In

the special case, unrealistic here, but appropriate for point obstacles, in which $\alpha << 1$ we find, independent of the value of T, that

$$\lambda = 1.41 / \alpha.$$

In comparison with the cases treated previously [1-3] there are additional complications: the obstacles have finite radius and; as we shall now see, have variable strengths as a consequence of having variable radii. Bacon ,Kocks and Scattergood [4] have shown through numerical studies that the Orowan stress, $\tau$, for a linear sequence of impenetrable circular blocks having radii a and inter-center spacings L is given by:

$$\tau = \frac{\mu\, b}{4\pi} \frac{\ln(\frac{X}{b})}{(L-2a)} = \mu b \sin\alpha,$$

where,

$$\frac{1}{X} = \frac{1}{2a} + \frac{1}{L}. \qquad (14)$$

In this expression, we have determined the breaking angle in the approximation (2) by equating the Orowan stress to that found numerically [5]. Thus, the specific strength of these obstacles is variable and, as we have supposed, can be denoted by the term:

$$\sin\alpha = \frac{\ln(X)}{4\pi}. \qquad (15)$$

This supposition may be justified from the observation [5] that, at breakaway, an obstructed dislocation, with symmetrical pinning, has

swept an area approximating that of a segment of a circle which subtends an angle $2\alpha$ at its center. That is to say, taken as a whole, the dislocation bends in much the same way as in the idealized model and thus into a circle of radius R, given by the relation:

$$R = \frac{\mu b}{\tau}.$$

The calculation of the yield strength for the circumstances specified here is complicated by three features. These are: the obstacles are not distributed along a straight line; they are not regularly spaced and; their strengths are variable. The consequences of the first two particulars have been considered in the foregoing, we now examine the effects of the variation in specific strength.

To progress we suppose, as indicated earlier, that the particles are spherical of radius r and that the concentration of the particulate phase is f. We then find that the mean spacing between particle centers in a slip plane is

$$L = \sqrt{\frac{2\pi}{3f}}\, r.$$

Again, the mean value of the radii of intersection of such a plane with the particles is readily found to be:

$$(\frac{2}{3})^{\frac{1}{2}} r.$$

Then towards the evaluation of the quantity $\sin \alpha$ as defined

in (15) we follow Friedel and suppose that at yield, dislocations are bent into arcs of circles of radius R such that the areas swept by the dislocation in circular segments between obstacles contain about one obstacle. Taking the critical angle turned by the dislocation at an obstacle as $2\theta$, the area of a swept segment is:

$$4R^2\theta^3/3.$$

Further,

$$\frac{4R^2\theta^3 f}{3} \sim \frac{(L-2a)^2\theta f}{3} = \frac{2\pi a^2}{3}.$$

Thence we see that

$$\frac{L-2a}{a} \sim \sqrt{\frac{2\pi}{f\theta}}$$

so that

$$L = a\,(2+\sqrt{\frac{\pi}{f\theta}}).$$

Thus, the mean value of the quantity X/b defined in (14) is

$$\frac{2a}{b}$$

provided, as is usually the case, $f\theta < \approx 0.1$, and (15) becomes:

$$\frac{\ln(\frac{2a}{b})}{4\pi} = \sin\alpha.$$

That is to say, in the circumstances considered here, the

strength of a particular obstacle of radius a is denoted by

$$\alpha \sim \sin \alpha = \frac{\ln \frac{2a}{b}}{4\pi}; \qquad (16)$$

An immediate consequence of the foregoing is that the radius R >>a since it is significantly larger than L unless $\theta > 60°$.

We are now in a position to consider the consequences of the simultaneous existence of obstacles of differing strengths. Reference to (12) and the realization that the analysis which proceeds it is essentially linear in the concentration of obstacles, shows that we may define a parameter $S_j$ for each group of obstacles characterized by a strength $\alpha_j$ and a concentration $c_j$ and then consider the quantity:

$$S_o = \frac{R^2 \sum_{j=1}^{m} C_j (e^{2\alpha_j T\lambda} - 1)}{\lambda (\lambda^2 T + 1)}$$

which in the limit of a continuous distribution of obstacle sizes becomes:

$$S_o = \frac{R^2}{\lambda (\lambda^2 T + 1)} \int_0^{\alpha_m} C(\alpha) (e^{2\alpha\lambda T} - 1) \, d\alpha. \qquad (17)$$

where $\alpha_m$ is the maximum strength of an obstacle, and $C_\alpha$ is the concentration of obstacles of strength $\alpha$.

In the case under consideration, where the particles are spherical and all of the same radius, r, it is easily shown that

the fraction, f(a) of circles of intersection of having radii in the range a to a +δa is

$$C(a)\,\delta a = \frac{a}{r\sqrt{r^2-a^2}}\delta a.$$

Then substituting for α in terms of a, (17) becomes:

$$S_0 = fr\frac{R^2}{4\pi r\lambda)}\int_0^r \frac{(\frac{2a}{b})^{\frac{(1+a/R)\lambda}{2\pi}}-1}{\sqrt{r^2-a^2}\ (\lambda^2(1+a/R)+1)}da,$$

where 2fr is the concentration of obstacles in a plane.

To progress we remember that a/R is small and see that this integral lies between lower and upper bounds. Thus,

$$\frac{fR^2}{8\lambda(\lambda^2+1)}\int_o^r \frac{(\frac{2a}{b})^{\frac{\lambda}{2\pi}}}{\sqrt{r^2-a^2}}da$$

$$<S_0$$

$$<\frac{fR^2(\frac{2a}{b})^{\frac{r}{2\pi R}}}{8\lambda(\lambda^2+1)}\int_0^r \frac{(\frac{2a}{b})^{\frac{\lambda}{2\pi}}}{\sqrt{r^2-a^2}}da. \qquad (18)$$

The integral of (18) can be expressed in terms of the Beta function. Thus, we find:

$$\int_0^r \frac{(\frac{2a}{b})^{\frac{\lambda}{2\pi}}}{\sqrt{r^2-a^2}}da = 2^{\frac{(\lambda-\pi)}{\pi}} r^{\frac{\lambda}{2\pi}} B(\frac{\lambda+2\pi}{4\pi}, \frac{\lambda+2\pi}{4\ \pi}) \equiv I \qquad (19)$$

The interpretation of this result is assisted by the use of the relation:

and Stirling's approximation:

$$B(x,y) = \frac{\Gamma(x)\Gamma(y)}{\Gamma(x+y)}$$

$$\Gamma(z) \sim 2\pi^{\frac{1}{2}}\, e^{-z}\, z^{z-\frac{1}{2}}.$$

Whence we find that (19) is:

$$I \sim \frac{2\pi\, 2^{(\frac{1}{2}-\frac{\lambda}{2\pi})}}{(\lambda+2\pi)^{\frac{1}{2}}}.$$

and that the inequality (18 ) becomes:

$$\frac{R^2\, C\, I^{\frac{\lambda}{2\pi b}}}{2\sqrt{\lambda+2\pi}\;\lambda(\lambda^2+1)}$$

$$< S_0$$

$$< \frac{R^2\, C\, I^{\frac{\lambda}{2\pi b}+\frac{r}{2\pi R}}}{2\sqrt{\lambda+2\pi}\;\lambda(\lambda^2+1)}$$

Inspection shows that these bounds are nearly coincident so that we may concentrate our attention on the simpler of the two.

Towards the determination of $\lambda$ we have as indicated earlier:

$$\frac{d\,\ln S_0}{d\lambda} = \frac{1}{S_0}\,\frac{dS_0}{d\lambda} = \frac{\sum_{i=1}^{n} \phi_i e^{\lambda\phi_i} p_i}{S_0} = \frac{\Phi}{N};$$

a quantity which tends to 0 as N tends to infinity. Accordingly differentiating with regard to $\lambda$ we find that we require and so from (20)

$$\frac{dS_0}{d\lambda} = 0$$

$$\frac{1}{2\pi} \ln\frac{r}{b} - \frac{1}{\lambda+2\pi} - \frac{2\lambda}{\lambda^2+1} - \frac{1}{\lambda} = 0.$$

In the range of interest in which

$$10^2 \leq \frac{2r}{b} \leq 10^5$$

we find that

$$2 \geq \lambda \geq 1.$$

Finally we require as a condition for yield that $S_0 = 1$. Accordingly setting

$$R = \frac{\mu b}{\sigma}$$

in (20 ) and substituting for C in terms of f we have

$$\sigma^2 = \frac{3\mu^2 b^2 f (\frac{2r}{b})^{\frac{\lambda}{2\pi}}}{4\pi\, r^2\sqrt{\lambda+2\pi}\;\lambda(\lambda^2+1)} \qquad (21)$$

Since $\lambda$ is largest when r is least we find that there is little variation in the term $(2r/b)^{\lambda/2\pi}$ with variation in $\lambda$. Overall, for a constant value of f, the yield stress varies nearly with the inverse of the particle size. It may be noted that Freidel's [6] conclusion that the yield stress varies with the square root of the concentration of point particles is retained to the situation where the particles have finite radius.

It may also be noted that using the relation:
(21) may be written in the more direct form:

$$L^2 = \frac{2\pi r^2}{3f},$$

$$\sigma^2 = \frac{\mu^2 b^2 \left(\frac{2r}{b}\right)^{\frac{\lambda}{2\pi}}}{L^2\sqrt{\lambda+2\pi}\ \lambda(\lambda^2+1)}.$$

Expressed in this way, we see that the yield stress varies essentially with the inverse of the mean particle spacing.

Conclusions:

An analytical treatment which proceeds on the same lines as those previously employed to evaluate the hardening effect of a dispersion of point obstacles has been used to deal with the case where the particles have finite radius. Qualitatively, the principal conclusions are that the predicted hardening should increase with the square root of the concentration of particulate phase and, for a fixed concentration, approximately with the inverse of the particle diameter. Further, the individual dependencies of strength on concentration and particle size can be subsumed into a single parameter: the inverse of the spacing between particle centers.

Acknowledgements:

This work has been supported by the Office of Naval Research under contract N00014-91-C-0067.

References:

1. Hanson, K. and Morris, J.W., J. Appl. Phys., 46, 983 (1975).

2. Labusch,R., J. Appl. Phys.,48, 4550 (1977).

3. Louat, N.P., ICSMA 5, 961 (1979).

4. Foreman, A.J.E. and Makin, M.J., Phil. Mag., 14, 911 (1966).

5. Bacon, D. J., Kocks, U.F. and Scattergood, R.O., Phil. Mag., 28, 1241 (1973).

6. Freidel, J., Les Dislocations, Gauthier- Villiers, Paris (1956).